Observing Plumes and Overturning Cells with a New Coastal Bottom Drifter

LENA M. SCHULZE CHRETIEN[a] AND KEVIN SPEER

Geophysical Fluid Dynamics Institute, Department of Earth, Ocean, and Atmospheric Science, Florida State University, Tallahassee, Florida

(Manuscript received 13 November 2017, in final form 26 June 2018)

ABSTRACT

A new platform, the Coastal Bottom Drifter, was designed and built to observe near-bottom environments in coastal regions. It is capable of observing properties by drifting near the bottom with a prescribed clearance or at a constant depth of up to 300 m. The platform can observe physical and biochemical parameters, such as temperature, salinity, oxygen, and velocities, and has the capacity to carry additional sensors to measure, for example, pH, turbidity, and nutrients. In addition, it can profile to the surface at chosen intervals and can be deployed for days or up to several months. The integrated Iridium communication allows the user to receive positions and data while the platform is surfaced, as well as send new missions to the instrument. The use of an acoustic bottom-tracking device allows the construction of a drifter trajectory while providing information about ocean circulation. Additionally, the ADCP provides information about suspended particles and possible sediment transport. These measurements are valuable in understanding coastal environments as well as the dominant physical processes that cause mixing and set the conditions for local biological activity. An example deployment in Apalachicola Bay shown in this study demonstrates the ability of the drifter to observe small-scale features, such as overturning cells and plumes of dense water, that are caused by local topography.

1. Introduction

Coastal zones are among the most dynamic and energetic environments, with strong wind-driven currents, waves, and tidal flows dominating the mixing of properties, organic matter, and sediments. Observing coastal processes is complicated with high variability resulting from strong forcing and large changes in stratification from the interaction between river and ocean sources in the presence of strong vertical and lateral mixing (Mei and Liu 1993).

Understanding the biogeochemistry of the continental shelf and coastal regions is important to assess the ecosystems and manage major coastal fisheries, as well as predict the carbon cycle (Jahnke et al. 2000; Gattuso et al. 2006). Many ecosystems, however, are undersampled, resulting in a bias toward less turbid, calmer sea state conditions (Jahnke et al. 2008), yet CO_2 budgets require ecosystem-specific projections, since they vary widely between habitats (Takeshita et al. 2015; Cai et al. 2011; Hofmann et al. 2011; Fassbender et al. 2011; Frieder et al. 2012). The lack of such measurements results in significant uncertainties in estimates of sea–air CO_2 fluxes over large areas (Takeshita et al. 2015) and shows the general need for near-bottom measurements in coastal environments to fully resolve the conditions in this region of the ocean (Jahnke et al. 2008).

Estuarine circulation, transport, and dynamics are often observed with moored instruments or ship-based measurements. These measurements include physical parameters, such as temperature and salinity, as well as biological and chemical measurements. Moored instruments have made a general understanding of the frequency spectrum of currents throughout the water column; unfortunately, these sampling strategies are often unable to provide the sampling needed to assess large variability in both space and time. While models often neglect detailed bottom topography and associated small-scale flow that is forced by topography, they provide an alternative way of investigating coastal dynamic and allow for interpretation and prediction of the environment (e.g., Chen et al. 2003; Liu and Huang 2009; Monismith and Fong 1996; Weisberg and Zheng 2006; Reed and Harrison 2016; Simons et al. 2010;

[a] Current affiliation: Marine Science Research Institute, Jacksonville University, Jacksonville, Florida.

Corresponding author: Lena M. Schulze Chretien, lschulz2@ju.edu

DOI: 10.1175/JTECH-D-17-0195.1

Huang et al. 2002; and many more). Satellite-tracked surface drifters (e.g., Manning et al. 2009; Ohlmann and Niiler 2005) allow for statistical representation of mean velocities, responding to wind events and preferred pathways. This approach, however, is limited to observing the surface currents, overlooking biological and chemical processes, as well as dynamics in the near-bottom environment. The last decade has brought many advances in ocean instrumentation, such as gliders and self-propelled vehicles [e.g., the Jetyak and Remote Environmental Monitoring Units (REMUS)], mooring technology (profiling and ice-detecting moorings), and profiling floats. While some instruments, such as ADCP's, are routinely deployed at fixed sites on the ocean floor, most autonomous vehicles and platforms are designed to avoid the bottom, since this region constitutes a greater danger for instruments.

Near-bottom environments are some of the most interesting and important zones for oceanographic dynamics, biological activity, and mixing. They are the location of intense interaction with internal waves, strong density currents and flows, hypoxic layers, and sediment and pollution pathways. These environments act as sinks of momentum while also being key zones of water mass transport (Thorpe 2005; Garrett et al. 1993). Enhanced mixing makes this region crucial for sediment transport (Grant and Madsen 1986) and transport of organic matter (Norcross and Shaw 1984; Todd 2013). The dynamics of near-bottom mixing remain unclear partly because of its highly variable nature and the difficulties of observing small-scale features with rapid time scales. The Coastal Bottom Drifter (CBD) presented in this paper is a new tool to investigate coastal systems specifically near and within the bottom boundary layer, giving insight into dynamics and biogeochemical conditions in this zone.

Below we will present the CBD and demonstrate its ability to fill a gap in observations of the near-bottom coastal environments. The CBD is capable of mapping variability on short time and spatial scales and over long time periods. It can obtain measurements continuously over large areas and under challenging conditions that make vessel operations impractical. In addition, autonomy and low operating costs compared to shipboard, mooring, or glider measurements make the platform an efficient tool for open-ocean and nearshore observations of dynamics and chemistry.

2. Drifter specifications and instrumentation

The CBD was designed by Florida State University (FSU) and fabricated by SeaScan, Inc. Its design allows the platform to drift near the bottom (presently at a maximum depth of 300 m) while measuring various parameters. The dimensions of the CBD are $111 \times 67.3 \times 60.2\,\text{cm}^3$ (Fig. 1) with a weight of 119 kg in air (see Table 1 for a detailed list of the weight).

The platform consists of an array of sensors that can collect oceanographic measurements 24/7 for days up to several months, depending on the configuration and battery demands of the instruments. It incorporates a Sea-Bird Scientific SBE 37 CTD with a dissolved oxygen sensor and an ADCP. Additional optical and biological sensors, such as chlorophyll, turbidity, pH sensor (and more), can be added. This is possible because of the extra available buoyancy (currently compensated by weights) that allows extra weight to be added. Sensors can be self-contained (with their own battery and memory) or be connected to the CBD battery and datalogger, which can be programmed to operate a wide range of instruments.

A central battery pack powers instruments that are connected to the datalogger, a Campbell Scientific CR1000, which also saves the collected data. Furthermore, the datalogger holds the dive missions for each deployment—a schematic for a possible dive mission is shown in Fig. 2—which can include several specific dive depths as well as bottom-tracking segments and surfacing periods. In addition to the dive mission, different emergency scenarios are programmed onto the CR1000, such as low or loss of battery, buoyancy engine failure, etc. In the case of a software-perceived emergency condition that prevents the CBD from surfacing, an emergency drop weight is released. Its release is expected to overcome some failure modes, and the platform should surface immediately. However, a new dive can be initiated only after the weight has been replaced.

The CBD's buoyancy engine enables the platform to dive to a given depth or to avoid the bottom by a predescribed clearance (Figs. 2 and 4) by checking the incorporated pressure sensor and altimeter, allowing the instrument to collect data close to the bottom even when the topography is changing. The buoyancy engine evaluates its position in the water column every 30 s by analyzing the statistics of depth, vertical velocity, and distance to the target depth over a 2-min period. An Iridium antenna provides GPS locations when the drifter surfaces and, additionally, allows the user to update missions and/or download data, as well as check the status of the CBD.

An acoustic tracking device [a Teledyne RD Instruments (RDI) Explorer Doppler velocity log (DVL) was used here but the CBD can be adapted for other devices, such as a NavQuest 600 Micro DVL] is attached to the bottom of the CBD. It is capable of measuring water profiles as well as velocities over the bottom and its distance to the bottom. The Explorer DVL is smaller,

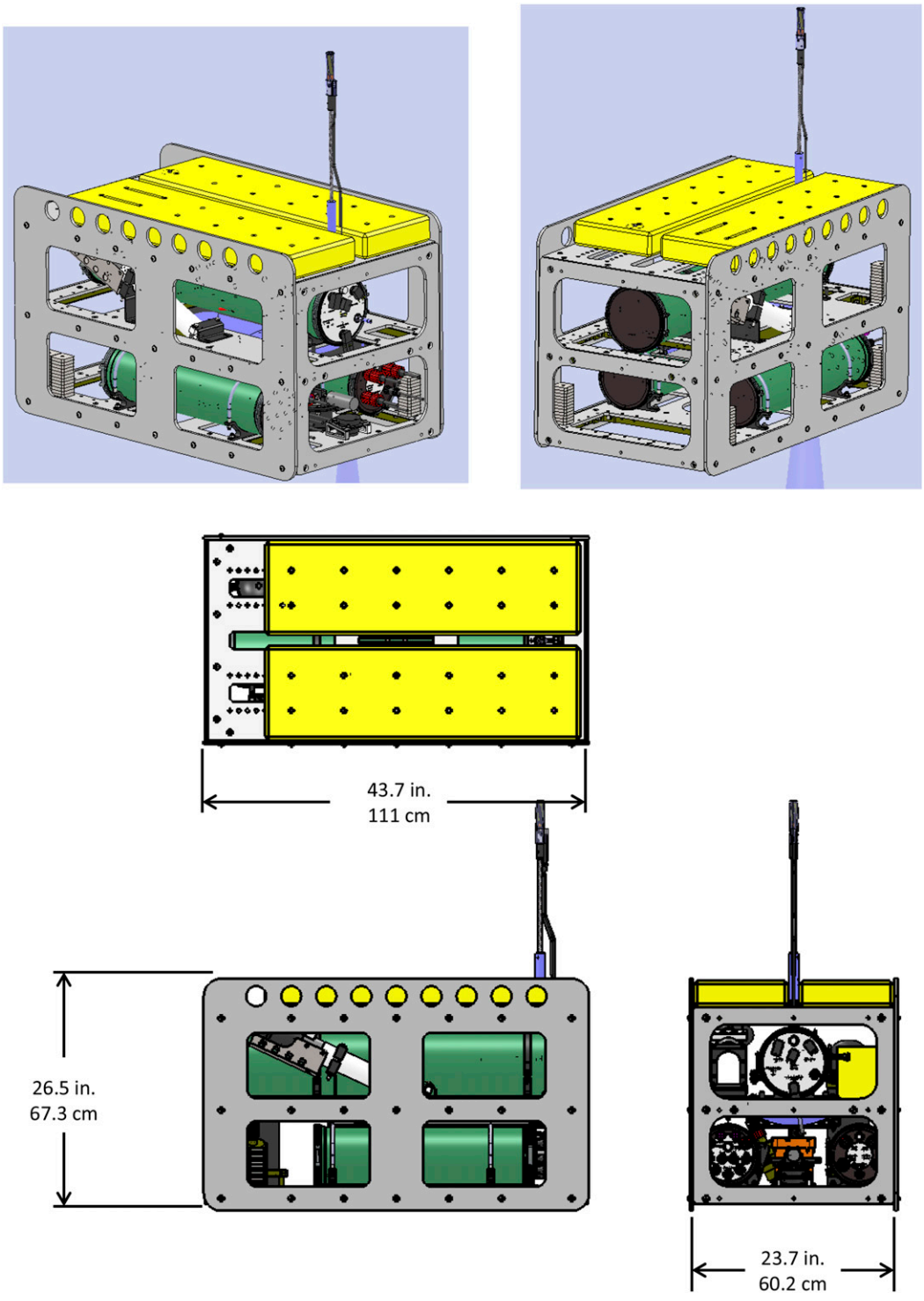

FIG. 1. Schematic drawing of the CBD. Courtesy of SeaScan, Inc.

weighs less, and provides a higher signal-to-noise ratio than bigger devices. These characteristics are due to its single-beam-forming phased-array transducer rather than the traditional individual piston transducers, making its measurements more precise in low-velocity environments. The ADCP can be purchased with an internal compass and attitude sensor (PNI Trax) that provides orientation information and is used to process the

TABLE 1. Weight and wet weight of major subassemblies of the CBD.

Description	Air weight (lb)	Wet weight (freshwater; lb)
Plastic frame with aluminum angle supports	87.9	23.8
Buoyancy engine assembly	51.8	−9.2
Battery housing assembly	33.5	2.43
Syntactic foam floatation	31.7	−49.9
Multiplexer science housing assembly	23.9	−6.9
Ballast weight	12	10.5
RDI ADCP and mounting bracket	10.4	1.5
Emergency drop weight assembly	13.2	10.75
Mineral oil	7.85	−0.97
External bladder assembly	6.6	2.3
Sea-Bird SBE 37	7.2	3.4
Underwater cables	3.2	1.5
Other	3	2

bottom velocity and velocity profiles. There are many examples of ADCPs that are attached to moving platforms (the most common one being shipboard ADCP data) and extensive literature on the processing of such data is available (e.g., Hummon and Firing 2003; Firing and Hummon 2010; Thurnherr et al. 2017). Since the CBD drifts relatively constant at one depth, the most important steps are a correction for its speed over the bottom, and pitch, roll, and heading. The onboard SBE 37 CTD O_2 sensor provides high-accuracy temperature, salinity, and dissolved oxygen data at the depth of the drifter when regularly calibrated.

3. Example of CBD diving missions

After the CBD is deployed, the instrument will start collecting data as programmed on the CR1000. Following the first dive command, it takes between 4 and 13 min for the CBD to submerge, depending on the stratification present at the deployment site. The CBD will settle to its given dive depth and adjust its buoyancy in 30-s intervals until receiving a new command from the CR1000. Two scenarios are possible: a dive to a specific depth or a bottom-following dive. For the first, the CBD will descend and stay at a given depth until receiving a new command. Should the given dive depth exceed the water depth, the drifter will automatically go into bottom-following mode and utilize the bottom clearance, until the water depth increases again or a new dive command is sent. For the second scenario, the CBD will follow the bottom topography with a given clearance

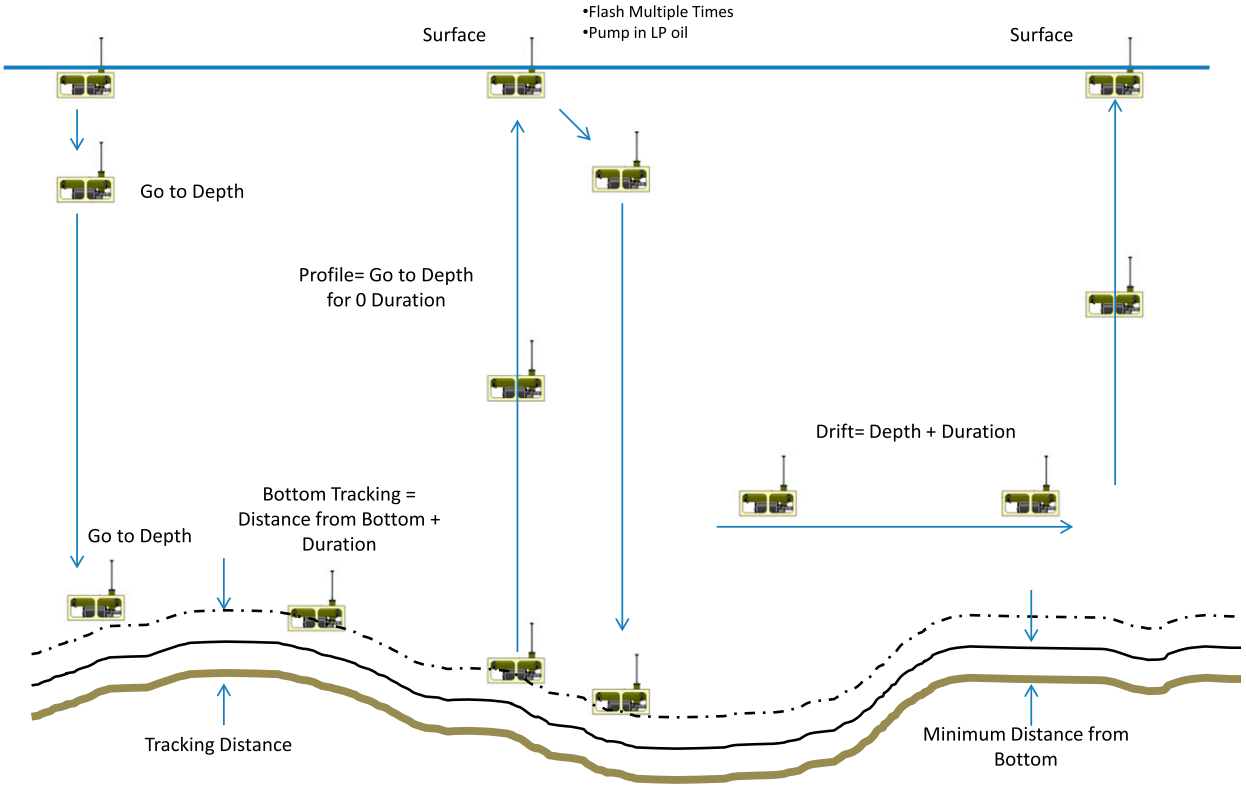

FIG. 2. Example of a possible CBD mission. Courtesy of SeaScan, Inc.

that can be as small as 2 m. The two dive modes allow the user to target specific regions of the water column, depending on the scientific objective.

Figure 3 shows an example of a dive mission to 10, 50, and 100 m. The first dive occurred at 1722 LT. The CBD quickly descended to 15 m but recovered to the set 10 m shortly after. During this recovery from 15 to 10 m, a new dive command was received (as seen by the gap in the blue line). This sent the CBD to 50 m, so it descended quickly without remaining at 10 m. The CBD oscillated around 50 m (correcting its buoyancy every 30 s to remain as close to the target depth as possible) but stayed within 1 m of the target depth. The third dive command was received at 1930 LT and sent the CBD to 100 m. Since the total water depth was only around 90 m, the CBD approached the bottom and followed the topography at its set clearance of 5 m (the red line in Fig. 3). Figure 4 shows another example of the CBD's bottom-tracking mode. Here, we show of a 2.5-h-long dive (during a different deployment) for which the CBD tracked the bottom of Apalachicola Bay with a clearance of 2 m. The CBD followed the topography closely, even for quick changes in the bottom depth (e.g., from 6.8 to 5.3 m at 2300–2309 LT).

When a surface command is sent to the buoyancy engine, the platform surfaces quickly within a couple of minutes, depending on its current depth. The fast ascend rate means that profiles of variables can only be measured with adequately high sampling rates. Sampling rates can be changed during the dive mission if required, by programming the CR1000 accordingly, to allow higher-resolution sampling during the profiling periods or while the CBD is close to the bottom.

As with any passive platform deployed in a semienclosed or coastal environment, grounding might be an issue. Some procedures have been implemented to prevent this scenario, the most important being the CBD's bottom avoidance feature described above. Should the drifter enter water that is shallower than 2 m, the instrument will no longer go into dive mode, in the hope that currents will carry it away from the shallow water into deeper water, where it can continue its dive missions. Should the CBD end up in a grounding situation, the user is able to assess the situation with use of the GPS positions sent through Iridium. Unfortunately, since the CBD is a passive instrument, there is not much that can be done if tides, currents, or waves do not free the instrument—the user will have to retrieve the platform and redeploy it in deeper water.

4. Drifter trajectories

GPS locations of the CBD, sent via the Iridium antenna, are available only while the platform is located at the surface. However, calculating the CBD position while underwater is possible when utilizing the CBD's u (east) and v (north) velocities over the bottom, which are collected by the ADCP, as well as the deployment position and GPS points collected during surfacing intervals.

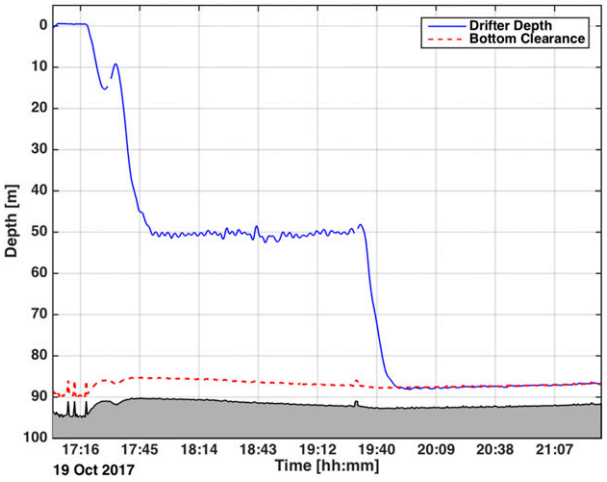

FIG. 3. Example of a dive. The actual depth of the CBD (blue line). The red broken line shows the 5-m bottom clearance that the CBD had to follow. Topography was obtained from the ADCP data.

We compare the calculated CBD trajectory to GPS positions obtained from a MetOcean beacon that was attached to the CBD predeployment for an 11-h period (2300 LT 18 May 2017–1000 LT 19 May 2017). The GPS trajectory shows an initial southward drift preceding a 10-h northwesterly drift (Fig. 5). To calculate a trajectory from the bottom velocities, we first average the velocities, which are collected every 30 s, onto a 2-min time vector and compare the angles of the drifter movement to the angles from the GPS data. We find that the angles calculated from the ADCP are on average 13.5° too large. We believe that a more elaborate calibration procedure will reduce this offset. After subtracting the compass offset from the ADCP dataset, the track obtained from the ADCP velocities agrees well with the track obtained from the GPS positions (Fig. 5). There is a slight deviation over time; however, this difference is only 265 m over the 11-h period and translates into a mean error velocity of 0.0067 m s^{-1}. This is smaller than the precision of the instrument recorded by RDI, which lies between 0.01 and 0.026 m s^{-1} at 1–5 m s^{-1}.

We split the CBD bottom velocities into low, medium, and fast speeds, and compare the offset between the GPS and CBD trajectory for these three regimes. With the mean speed of 0.18 m s^{-1} over the 11-h period, the low regime is defined to be speeds lower than 0.15 m s^{-1}, the midrange are speeds between 0.15 and 0.2 m s^{-1}, and speeds in the fast regime must exceed 0.2 m s^{-1}. Of the 330 velocity points, 35.5% are in the low regime, 34.5%

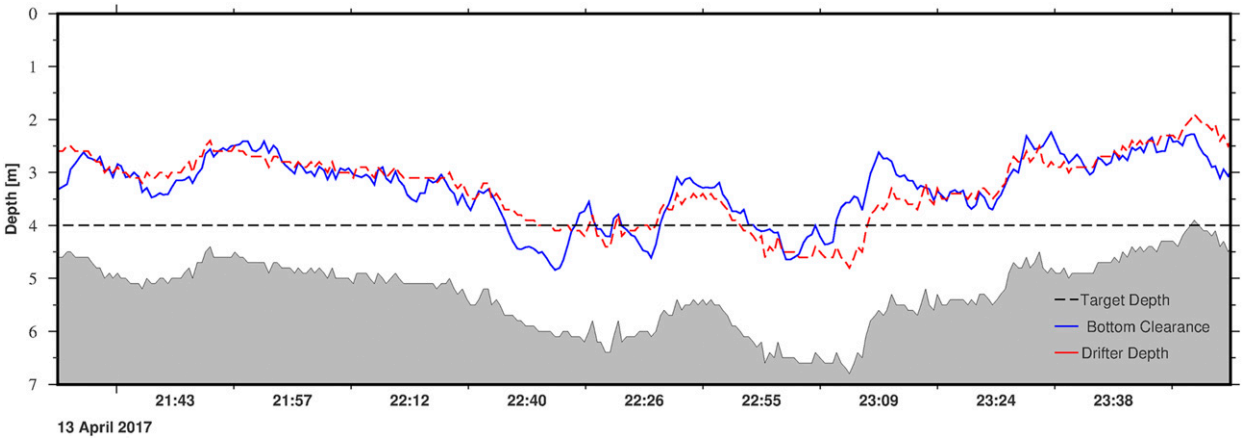

FIG. 4. Example of the drifter's bottom avoidance feature showing the 2-m clearance (blue line) and the depth of the drifter (red line). The black broken line shows the dive depth that was given to the CBD. Topography was obtained from the ADCP data.

are in the midrange, and 30% are in the fast regime. When calculating the difference for the tracks of each regime compared to the GPS track, we find that the difference is 111.7 m for the low velocities, 166.1 m for the midrange velocities, and 200.8 m for the track from the fastest velocities. In other words, when the CBD is moving with speeds below 0.15 m s^{-1}, the error of the trajectory is half that compared to speeds above 0.2 m s^{-1}. This is in line with the decrease in precision with increasing velocities recorded by RDI (http://www.teledynemarine.com/Lists/Downloads/explorer_datasheet_hr.pdf).

5. Observations of circulation in Apalachicola Bay

Apalachicola Bay is a barrier island estuarine system running in the east–west direction along the Florida Panhandle. The bay is on average about 3 m deep but has several regions where the water can be as deep as 8–20 m. A periodic change of water level and properties is caused mainly by the diurnal and semidiurnal tidal components (Jones and Mozo 1993, 1994), but surface winds can also play a significant role in the volume exchange between the bay and the Gulf, as well as the salinity variations within the bay (Huang et al. 2002). Apalachicola Bay is highly productive and supports an abundant variety of commercial and noncommercial fish and shellfish. The well-being of the shellfish is directly proportional to the salinity (Livingston et al. 2000) and sediments (Liu and Huang 2009; Volety and Encomio 2006) in the bay. For example, an increase of suspended sediment can reduce light availability, affecting algal and aquatic vegetation growth (Blom et al. 1994).

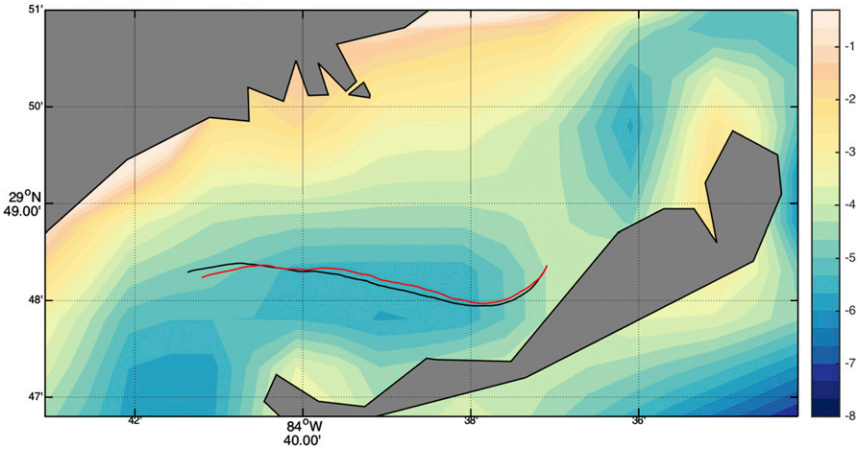

FIG. 5. Example of tracking the drifter using the ADCP bottom track velocities. The trajectory from the Iridium GPS locations (blue line). The red trajectory was calculated using the ADCP's velocity over the bottom and the first GPS point as a start point. The bottom topography was obtained from Etopo.

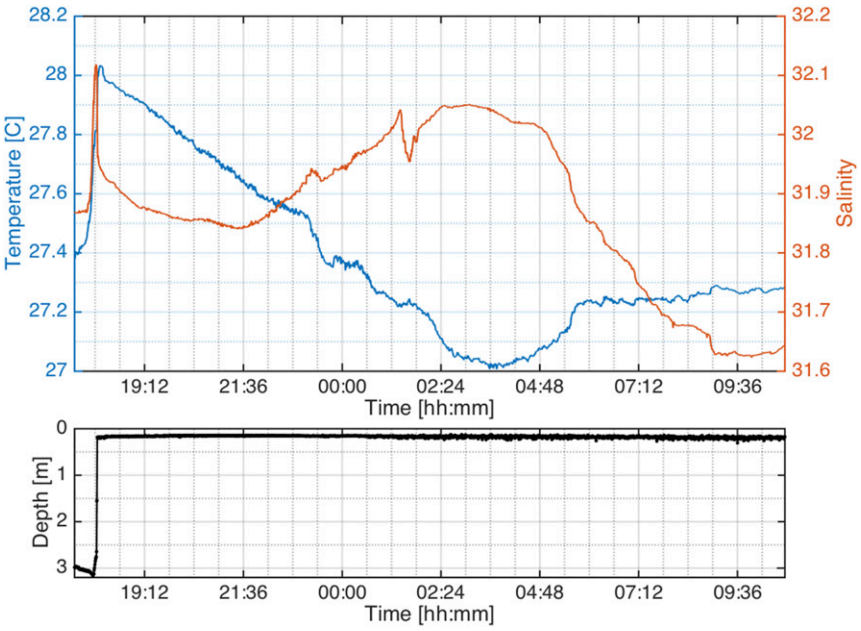

FIG. 6. (top) Temperature (blue) and salinity (orange) measured by the SBE 37 on the drifter. (bottom) Pressure at which the temperature and salinity in the top panel were measured.

The major freshwater input into the bay comes from the Apalachicola River with an annual average flow of 670 $m^3 s^{-1}$ (Dulaiova and Burnett 2008), but model studies suggest that strong and steady winds can transport as much as 2000 $m^3 s^{-1}$ of saline water into the bay or flushing freshwater out of the bay depending on the wind direction (Huang et al. 2002), causing large variability and flushing times between 6 and 12 days (Dulaiova and Burnett 2008). This makes it challenging to observe and forecast the bay conditions with traditional instrumentation and hence predict the impact of changes on shellfish and the fisheries.

For the purpose of demonstrating the CBD's ability to serve as a new observation platform capable of observing highly variable coastal systems, we present data from an 18-h-long deployment (from 1700 LT 18 May 2017 to 1045 LT 19 May 2017) in Apalachicola Bay (the same deployment mentioned in section 4). During the deployment the CBD was drifting at the surface with the exception of the first hour, during which it was diving at a depth of around 3 m. The deployment included measurements of temperature, salinity (Fig. 6), dissolved oxygen (not shown), and velocity profiles (Fig. 7) collected every 30 s. Each velocity profile consisted of a set of 100 pings in 30-cm bins. The bottom depth was calculated from the ADCP data and is shown in Figs. 7–9. The tides at the time and location of the deployment had a magnitude of around 0.6 m. High tide occurred at 1940 LT 18 May (with a height of 0.61 m) and 1043 LT 19 May (with a height of 0.52 m), and low tide was observed at 0332 LT 19 May (with a height of 0.06 m).

The CTD shows cold and freshwater at the depth of 3 m. Both increase rapidly after the first hour of the deployment, during the CBD's ascent to the surface. The CTD sampling rate was 30 s, which resulted in coarse sampling of the water column during the quick ascent (with several measurements between 3 and 2.8 m, one at 1.5 m, before reaching the surface). The water temperature at the surface was 28°C but decreased steadily over a 5-h period (until about 0000 LT) and then more rapidly over another 4.4 h, until reaching 27°C at 0330 LT. The minimum in temperature coincided with the tidal low. Salinity decreased rapidly after the initial surfacing, from 32.1 to 31.95 and then slower to 31.85. At around 2200 LT salinities started increasing again, reaching a maximum just before 0330 LT. This maximum coincides with the temperature minimum and low tide. After this, until 0930 LT salinities decreased to 31.6, while temperatures remained at around 27.5°C after a brief increase. Small variations present in salinity, such as a quick and short freshening period around 0130 LT, are not present in temperature. In addition, the pressure time series is very smooth until around 0100 LT, showing strong variance after that until the end of the deployment.

For a full picture of the circulation and to better understand what role tides and winds might play in forcing the observed temperature and salinity changes, we analyze the velocity profiles obtained by the ADCP. We show velocities that were smoothed onto a 2-min grid, but all features discussed are also present in the original

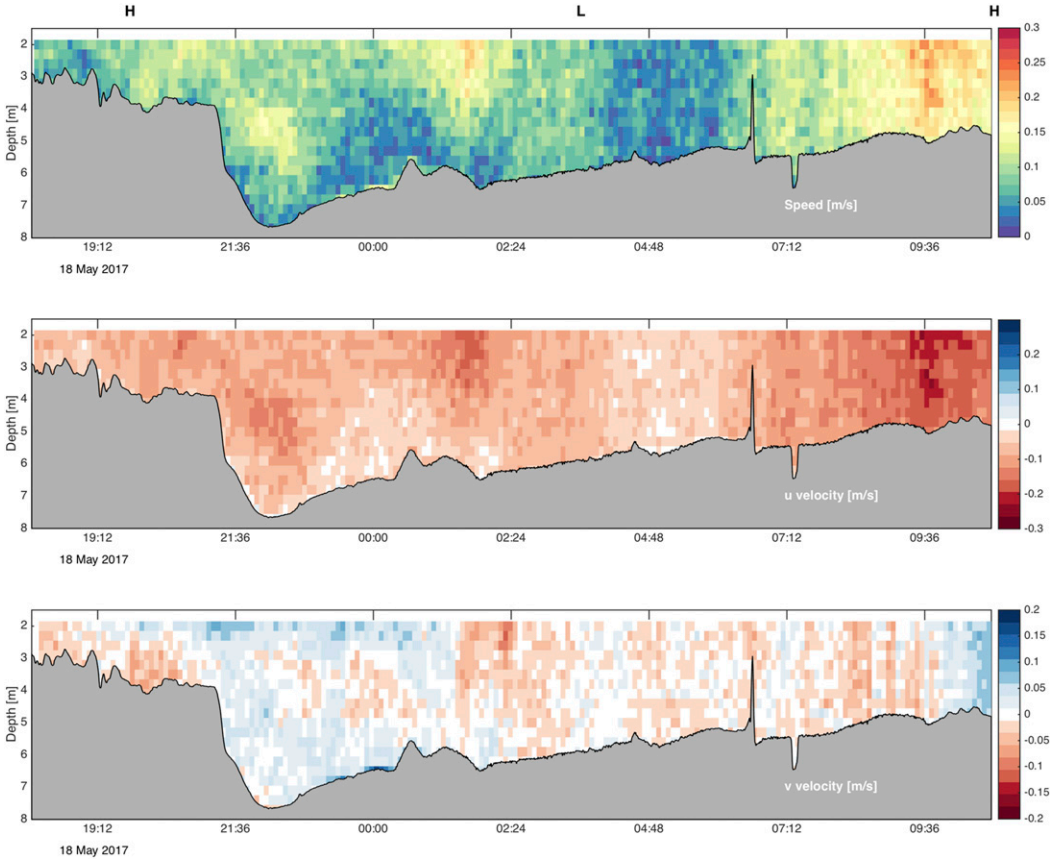

FIG. 7. (top) Speed ($m\,s^{-1}$) obtained from the ADCP data. (middle) The u velocity ($m\,s^{-1}$) obtained by the ADCP. All positive velocities (blue shading) are east, while negative velocities (red shading) are westward. (bottom) As in the middle panel, but for the v velocities. All positive v velocities (blue shading) are oriented to the north, while negative velocities (red shading) are oriented to the south. For all three panels, the shown bottom topography was calculated by the ADCP. The H and L show the timing of the high and low tides, respectively.

30-s data. The drift of the CBD was dominated by the u velocity throughout the entire deployment (also seen from the trajectories in Fig. 5). At the time of the first high tide, the drifter was located in water of 3–4 m, moving slowly with $0.07\,m\,s^{-1}$. Shortly after the high tide, the speed as well as u and v increased and were characterized by shear between the upper meter and lower 3 m, though the shear was strongest in the v component. At the same time, the u velocities and speed showed a surface-intensified flow that corresponds to increased downward velocities (seen in the vertical velocities; Fig. 8). The eddy kinetic energy (EKE), often taken to be a rough measure of turbulence, was not elevated at this point. Instead, it showed signs of increased mixing earlier, just before the high tide, at 1900 LT, while speeds and the u velocities were low.

Around 2130 LT the bottom depth changed quickly from 4 to 8 m, and the u velocity component reached speeds of $0.17\,m\,s^{-1}$, with a maxima at 5 m. Downward motion was still present at this time throughout the 8 m of water and especially near the slope and below 4 m (Fig. 8a). This indicates that water from the shallow sill spilled into the region of deeper water. The overflow was composed of dense water from the Gulf of Mexico. Additional evidence of this dense plume comes from a tail of high backscatter along the slope (Fig. 9). The core of the deep westward flow (seen in the u velocities) is associated with enhanced EKE. Hence, the region of deeper water and its deep flow are associated with increased mixing and turbulence. At the same time, it coincides with the beginning of increasing surface salinities around 2200 LT, indicating that the increased mixing at depth impacts the surface salinity by mixing salty water toward the surface.

What, then, caused the notable decrease of surface temperatures that started at 0000 LT? Recall that temperatures decreased steadily until 0000 LT before a more rapid and less linear decrease between 0000 and 0330 LT. This change coincides with the ebbing before the low tide at 0330 LT. However, we do not believe that

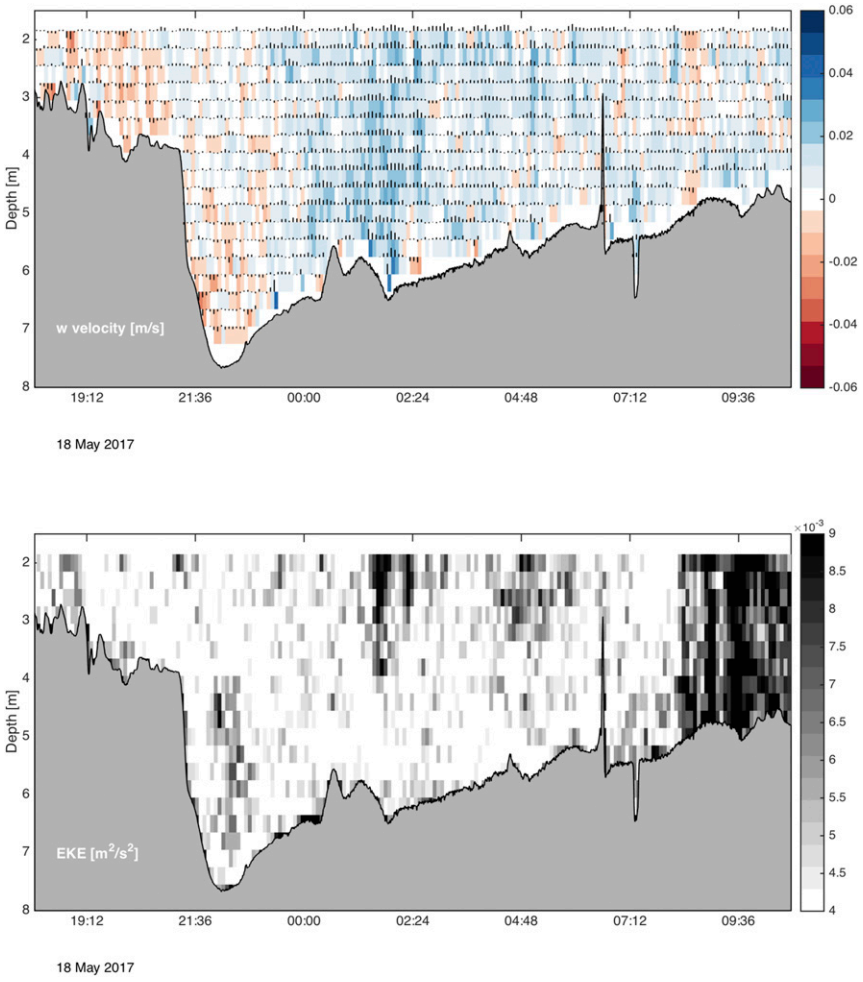

FIG. 8. (top) Vertical velocities ($m\,s^{-1}$) obtained from the ADCP. Black bars in each depth cell show the direction and strength of the vertical velocities. Colors denote upwelling (blue shading) and downward motion (red shading). (bottom) The EKE ($m^2\,s^{-2}$) calculated from u and v of the ADCP data. Darker shading shows higher levels of variability. For both panels, the displayed bottom topography was calculated by the ADCP.

the temperature change was caused by the ebbing but rather interpret it as being due to the presence of a strong overturning cell together with strong surface winds. At 0000 LT, the recorded 10-m wind speeds, measured at the FSU Marine Laboratory, suddenly increased from 2 to 14 $m\,s^{-1}$, persisting over a period of 3 h before slowing (Fig. 10). This coincided with intense upwelling of salty and cold water. The upwelling is also visible in the form of low backscatter that extends from the bottom (at around 6–7 m) upward into the surface layer (Fig. 9) and was associated with relatively low speeds and EKE (Fig. 8). Just 1.5 h later (at 0130 LT) the CBD encountered a surface-intensified flow that likely transported the upwelled cold and salty water away from the site. The presence of the jet coincided with a short period of surface freshening at 0130 LT that was mentioned earlier. Hence, not only did the intensified surface flow flush away the salty and cold water, but it also brought fresh and slightly warmer water to the site.

During low tide (0330 LT), remnant upward motion in the upper half of the water column was observed. However, overall the water column was characterized by low velocities and little mixing, as evident in the low EKE and strong gradient of backscatter throughout the water column. Shortly after, EKE increased at the surface. Backscatter remained high at the surface but the vertical gradient decreased, with higher backscatter reaching from the surface to 5 m. Interestingly, while the EKE at the surface was similar to the signal observed in the surface jet at 0130 LT, velocities here were low throughout the water column, increasing only at 0700 LT, during the flooding period. This points to a

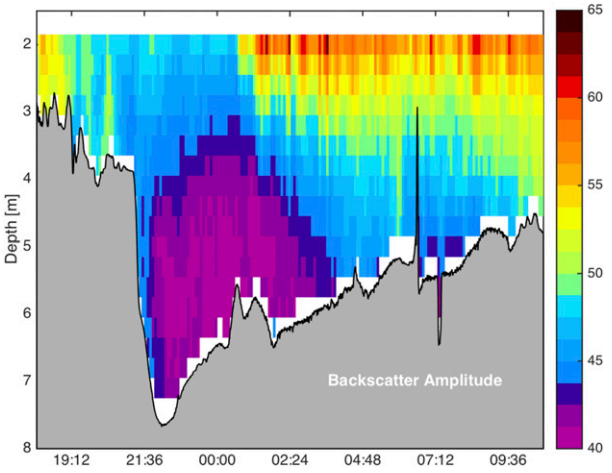

FIG. 9. Backscatter amplitude obtained from the ADCP. The displayed bottom topography was calculated by the ADCP.

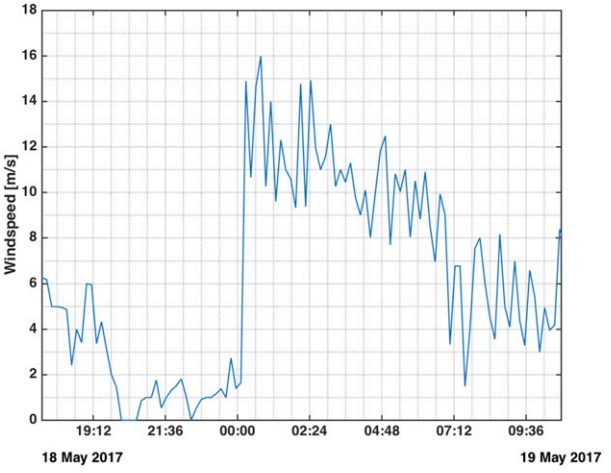

FIG. 10. Wind speed at 10-m height, measured at FSU Marine Laboratory, around 13 km away from the drifter deployment site.

different forcing/mechanism causing the turbulence than during the earlier period. The strongest velocities, reaching 0.24 m s^{-1}, were observed at around 0930 LT and were associated with the flood phase of the tidal cycle that is also evident in the steadily decreasing salinities between 0330 and 0930 LT.

Recall that the CTD pressure time series (Fig. 6) showed increased variability starting at 00:30 LT. We interpret this as increased up and down movement of the CBD starting protocol. The timing of this variability coincides with the first surface jet (Fig. 7) as well as the upwelling seen in the vertical velocities (Fig. 8). However, the turbulence observed in the CTD pressure lasted until the end of the deployment compared with the shorter surface jet and upwelling periods. The increased surface backscatter coincides closely with the variability in pressure (Fig. 9). Backscatter such as this is usually attributed to advection of air microbubbles produced by surface wave breaking resulting from strong forcing, such as larger wind stress (Zedel and Farmer 1991). This is consistent with the storm that swept through the region starting at midnight (Fig. 10). Hence, the high backscatter at the surface and the movement of the CBD, apparent in the variability of the pressure, indicated a rough sea state in Apalachicola Bay during this time period.

6. Summary and discussion

A new coastal bottom drifter was tested over a period of two years. Following numerous pool tests, the CBD was deployed in the ocean for periods up to 24 h at a time. These deployments include six in Apalachicola Bay to test the diving and changes to the mission code. One of these longer deployments was designed specifically to test the bottom-tracking capabilities (Fig. 4), another is the subject of this report. Two additional tests were conducted offshore in about 100 m of water, lasting about 6 h (Fig. 3).

In this paper we present data from a deployment of the CBD over an 18-h period in May 2017 in Apalachicola Bay. It was able to observe some unique dynamics that were driven not only by tidal mixing but also by wind forcing and the presence of dense water from the Gulf of Mexico. In particular, the CTD showed a temperature change of 1°C over a 9-h period that was caused by tides as well as an overturning cell. Salinity varied between 31.62 and 32.1 with changes caused by tides, the overturning cell, and a surface jet that brought fresher water into the path of the CBD. The high-resolution ADCP was able to provide a highly accurate bottom track and high-resolution velocity data in the u, v, and w directions. The velocities showed overflow of dense water from the Gulf of Mexico combined with a deeper westward jet. Turbulence, as indicated by velocity shear and EKE, was elevated at this location. Only 2.5 h later the vertical velocities as well as the backscatter showed an overturning cell caused by wind that impacted the surface temperature and salinity.

The CBD is a novel instrument capable of observing high-variability changes in coastal regions. Its ability to detect the bottom and measure the environmental conditions there makes it a unique platform for a wide range of applications, including observing physical mechanisms and associated biochemical systems. Studies have, for example, given some insight about the connection of water budgets for heat and salt as well as chemistry (Axell 1998; Gustafsson and Stigebrandt 2007; Holtermann et al. 2012; Holtermann and Umlauf 2012), but the methods

have large uncertainties because of model assumptions. The CBD could measure these variables as well as velocity shear in the near-bottom environments for several weeks and investigate diapycnal mixing on longer time scales and in specific areas, possibly combined with tracer releases or microstructure measurements. It fills an observational gap with the ability to dive close to the bottom purposefully, follow the uneven bottom topography, and measure flow and hydrography in the boundary layer. Dive missions may be adapted to the needs of sampling and the geographic complexity.

Acknowledgments. This project is funded through the Ocean Technology Development Grant from NOAA, PTE Federal Award Number NA15OAR4320064. We also would like to thank the captain and crew of the R/V *Apalachee* and the Twin V for helping with the deployments and tests of the CBD.

REFERENCES

Axell, L., 1998: On the variability of Baltic Sea deepwater mixing. *J. Geophys. Res.*, **103**, 21 667–21 682, https://doi.org/10.1029/98JC01714.

Blom, G., E. H. S. van Duin, and L. Lijklema, 1994: Sediment resuspension and light conditions in some shallow Dutch lakes. *Water Sci. Technol.*, **30**, 243–252, https://doi.org/10.2166/wst.1994.0534.

Cai, W.-J., and Coauthors, 2011: Acidification of subsurface coastal waters enhanced by eutrophication. *Nat. Geosci.*, **4**, 766–770, https://doi.org/10.1038/ngeo1297.

Chen, C., H. Liu, and R. Beardsley, 2003: An unstructured grid, finite-volume, three-dimensional, primitive equations ocean model: Application to coastal ocean and estuaries. *J. Atmos. Oceanic Technol.*, **20**, 159–186, https://doi.org/10.1175/1520-0426(2003)020<0159:AUGFVT>2.0.CO;2.

Dulaiova, H., and W. Burnett, 2008: Evaluation of the flushing rates of Apalachicola Bay, Florida via natural geochemical tracers. *Mar. Chem.*, **109**, 395–408, https://doi.org/10.1016/j.marchem.2007.09.001.

Fassbender, A., C. Sabine, R. Feely, C. Langdon, and C. Mordy, 2011: Inorganic carbon dynamics during northern California coastal upwelling. *Cont. Shelf Res.*, **31**, 1180–1192, https://doi.org/10.1016/j.csr.2011.04.006.

Firing, E., and J. Hummon, 2010: Shipboard ADCP measurements. GO-SHIP repeat hydrography manual: A collection of expert reports and guidelines, IOCCP Rep. 14, ICPO Publ. Series 134, Version 1, 11 pp.

Frieder, C. A., S. H. Nam, T. R. Martz, and L. A. Levin, 2012: High temporal and spatial variability of dissolved oxygen and pH in a nearshore California kelp forest. *Biogeosciences*, **9**, 3917–3930, https://doi.org/10.5194/bg-9-3917-2012.

Garrett, C., P. MacCready, and P. Rhines, 1993: Boundary mixing and arrested Ekman layers: Rotating stratified flow near a sloping boundary. *Annu. Rev. Fluid Mech.*, **25**, 291–323, https://doi.org/10.1146/annurev.fl.25.010193.001451.

Gattuso, J.-P., B. Gentili, C. M. Duarte, J. A. Kleypas, J. J. Middelburg, and D. Antoine, 2006: Light availability in the coastal ocean: Impact on the distribution of benthic photosynthetic organisms and their contribution to primary production. *Biogeosciences*, **3**, 489–513, https://doi.org/10.5194/bg-3-489-2006.

Grant, D., and O. Madsen, 1986: The continental-shelf bottom boundary layer. *Annu. Rev. Fluid Mech.*, **18**, 265–305, https://doi.org/10.1146/annurev.fl.18.010186.001405.

Gustafsson, B. G., and A. Stigebrandt, 2007: Dynamics of nutrients and oxygen/hydrogen sulfide in the Baltic Sea deep water. *J. Geophys. Res.*, **112**, G02023, https://doi.org/10.1029/2006JG000304.

Hofmann, G., and Coauthors, 2011: High-frequency dynamics of ocean pH: A multi-ecosystem comparison. *PLoS ONE*, **6**, e28983, https://doi.org/10.1371/journal.pone.0028983.

Holtermann, P., and L. Umlauf, 2012: The Baltic Sea Tracer Release Experiment: 2. Mixing processes. *J. Geophys. Res.*, **117**, C01022, https://doi.org/10.1029/2011JC007445.

——, ——, T. Tanhua, O. Schmale, G. Rehder, and J. Waniek, 2012: The Baltic Sea Tracer Release Experiment: 1. Mixing rates. *J. Geophys. Res.*, **117**, C01021, https://doi.org/10.1029/2011JC007439.

Huang, W., W. Jones, and T. Wu, 2002: Modelling wind effects on subtidal salinity in Apalachicola Bay, Florida. *Estuarine Coastal Shelf Sci.*, **55**, 33–46, https://doi.org/10.1006/ecss.2001.0881.

Hummon, J., and E. Firing, 2003: A direct comparison of two RDI shipboard ADCPS: A 75-khz ocean surveyor and a 150-khz narrow band. *J. Atmos. Oceanic Technol.*, **20**, 872–888, https://doi.org/10.1175/1520-0426(2003)020<0872:ADCOTR>2.0.CO;2.

Jahnke, R. A., J. R. Nelson, R. L. Marinelli, and J. E. Eckman, 2000: Benthic flux of biogenic elements on the Southeastern US continental shelf: Influence of pore water advective transport and benthic microalgae. *Cont. Shelf Res.*, **20**, 109–127, https://doi.org/10.1016/S0278-4343(99)00063-1.

——, ——, M. E. Richards, C. Y. Robertson, A. M. F. Rao, and D. B. Jahnke, 2008: Benthic primary productivity on the Georgia midcontinental shelf: Benthic flux measurements and high-resolution, continuous in situ PAR records. *J. Geophys. Res.*, **113**, C08022, https://doi.org/10.1029/2008JC004745.

Jones, W., and M. Mozo, 1993: Apalachicola Bay freshwater needs assessment program, geophysical data collection program. Vol. 1, Northwest Florida Water Management District Water Resources Special Rep. 93-5.

——, and ——, 1994: Apalachicola Bay freshwater needs assessment program, geophysical data collection program. Vol. 2–4, Northwest Florida Water Management District Water Resources Special Rep. 94, 110 pp.

Liu, X., and W. Huang, 2009: Modelling sediment resuspension and transport induced by storm wind in Apalachicola Bay, USA. *Environ. Modell. Software*, **24**, 1302–1313, https://doi.org/10.1016/j.envsoft.2009.04.006.

Livingston, R., and Coauthors, 2000: Modelling oyster population response to variation in freshwater input. *Estuarine Coastal Shelf Sci.*, **50**, 655–672, https://doi.org/10.1006/ecss.1999.0597.

Manning, J. P., D. J. McGillicuddy Jr., N. R. Pettigrew, J. H. Churchill, and L. S. Incze, 2009: Drifter observations of the Gulf of Maine coastal current. *Cont. Shelf Res.*, **29**, 835–845, https://doi.org/10.1016/j.csr.2008.12.008.

Mei, C., and P. Liu, 1993: Surface waves and coastal dynamics. *Annu. Rev. Fluid Mech.*, **25**, 215–240, https://doi.org/10.1146/annurev.fl.25.010193.001243.

Monismith, S. G., and D. A. Fong, 1996: A simple model of mixing in stratified tidal flows. *J. Geophys. Res.*, **101**, 28 583–28 595, https://doi.org/10.1029/96JC02267.

Norcross, B. L., and R. F. Shaw, 1984: Oceanic and estuarine transport of fish eggs and larvae. *Trans. Amer. Fish. Soc.*, **113**, 155–165, https://doi.org/10.1577/1548-8659(1984)113<153:OAETOF>2.0.CO;2.

Ohlmann, J., and P. Niiler, 2005: Circulation over the continental shelf in the northern Gulf of Mexico. *Prog. Oceanogr.*, **64**, 45–81, https://doi.org/10.1016/j.pocean.2005.02.001.

Reed, D., and J. Harrison, 2016: Linking nutrient loading and oxygen in the coastal ocean: A new global scale model. *Global Biogeochem. Cycles*, **30**, 447–459, https://doi.org/10.1002/2015GB005303.

Simons, R., S. Monismith, F. Saucier, L. Johnson, and G. Winkler, 2010: Modelling stratification and baroclinic flow in the estuarine transition zone of the St. Lawrence estuary. *Atmos.–Ocean*, **48**, 132–146, https://doi.org/10.3137/OC316.2010.

Takeshita, Y., and Coauthors, 2015: Including high-frequency variability in coastal ocean acidification projections. *Biogeosciences*, **12**, 5853–5870, https://doi.org/10.5194/bg-12-5853-2015.

Thorpe, S., 2005: *The Turbulent Ocean*. Cambridge University Press, 439 pp.

Thurnherr, A., I. Goszczko, and F. Bahr, 2017: Improving LADCP velocity with external heading, pitch, and roll. *J. Atmos. Oceanic Technol.*, **34**, 1713–1721, https://doi.org/10.1175/JTECH-D-16-0258.1.

Todd, A. C., 2013: Circulation dynamics and larval transport mechanisms in the Florida Big Bend. Ph.D. dissertation, Florida State University, 90 pp.

Volety, A. K., and V. G. Encomio, 2006: Biological effects of suspended sediments on shellfish in the Charlotte Harbor Watershed—Implications for water releases and dredging activities. Florida Gulf Coast University Final Rep., 47 pp.

Weisberg, R. H., and L. Y. Zheng, 2006: Circulation of Tampa Bay driven by buoyancy, tides, and winds, as simulated using a finite volume coastal ocean model. *J. Geophys. Res.*, **111**, C01005, https://doi.org/10.1029/2005JC003067.

Zedel, L., and D. Farmer, 1991: Organized structures in subsurface bubble clouds: Langmuir circulation in the open ocean. *J. Geophys. Res.*, **96**, 8889–8900, https://doi.org/10.1029/91JC00189.